X-Ray–Line Diagnostic of Magnetic Field Strength for High-Temperature Plasmas

P. Beiersdorfer, J. H. Scofield, and A. L. Osterheld

Department of Physics and Advanced Technologies, Lawrence Livermore National Laboratory, Livermore, California 94550, USA

(Received 19 March 2002; published 13 June 2003)

An x-ray line diagnostic for use in magnetic field measurements in high-temperature plasmas has been identified. The intensity of the otherwise strictly forbidden $1s^2 2s^2 2p_{1/2} 2p_{3/2}^4 3s_{1/2}\ ^3P_0 \rightarrow 1s^2 2s^2 2p^6\ ^1S_0$ transition in neonlike ions is shown to depend on the magnetic field strength. The field dependence is illustrated between one and 3 T in the Ar^{8+} spectrum. The line is well resolved, bright, and close to reference lines, making it an experimentally simple to use diagnostic.

DOI: 10.1103/PhysRevLett.90.235003 PACS numbers: 52.70.La, 32.30.Rj, 32.60.+i, 32.70.Fw

The magnetic field strength is a crucial plasma parameter. Even relatively weak fields in kinetic terms, i.e., magnetic field pressure $\ll$ plasma kinetic pressure, are important for determining particle and energy transport and thus plasma confinement. Magnetic field measurements using the Zeeman effect of optical lines from neutrals or singly charged ions in the photosphere have revealed fields in excess of 4 kG [1]; measurements and magnetospheric accretion models even predict fields in excess of 1 T (10 000 G) for other types of stars [2]. Yet higher magnetic fields are predicted in laser-produced and *Z*-pinch plasmas. Polarimetry measurements of probe laser pulse or self-generated laser harmonics revealed fields as high as 34 000 T in laser-matter interactions [3,4].

For a large number of plasmas no magnetic field measurements are possible. In many cases, the use of external radiation to measure magnetic fields is impossible. Moreover, in high-temperature plasma where ions attain high charge states and radiate in the EUV and x-ray range, magnetic field determinations from the Zeeman splitting of lines from neutrals or singly charged ions are often no longer possible. X-ray lines provide accurate information on temperature and density [5–10], for example, but so far none provide any direct information on the magnetic field strength.

In the following we close this gap in the diagnostic utility of x-ray lines by demonstrating the sensitivity of the strictly forbidden $(1s^2 2s^2 2p_{1/2}^5 3s_{1/2})_{J=0}\ ^3P_0 \rightarrow (1s^2 2s^2 2p^6)_{J=0}\ ^1S_0$ transition in the neonlike ion to the magnetic field strength. In a low-density environment, neonlike sulfur, argon, or iron can provide the magnetic field strength from a few hundred gauss to up to a few tesla, and thus can cover the range of field strengths expected, for example, in many stellar atmospheres. In a high-density environment, the diagnostic is useful for estimating the magnetic field strength as high as several thousand T depending on the value of the electron density.

Emission optical magnetic field diagnostics are based on line broadening (or splitting) caused by removing the energy degeneracies of a given fine structure level in the presence of an external magnetic field [11,12]. Magnetic fields also remove the degeneracy of the levels connecting a given x-ray transition. But the resulting broadening is generally too small to measure and is masked by other line broadening mechanisms. The principle of our diagnostic is based instead on the fact that the magnetic field resolves the degeneracy of the magnetic sublevels of a given level and allows mixing with sublevels of a neighboring level as long as they have the same magnetic quantum number and parity, i.e., the wave function describing a given level assumes components from that of a neighboring level. In other words, the appearance of nondegenerate magnetic sublevels enables the mixing of quantum levels that in the field-free case could not interact because this would involve levels with different total angular momentum. Magnetic field mixing in many cases is irrelevant, as it typically is weak, and both levels are likely to have strong radiative decay channels, i.e., a few parts per million change in the radiative decay rates will hardly be noticeable given the present accuracy of calculations and measurements. However, if one of the levels has no or only a very weak radiative channel while the other has a strong radiative decay channel, magnetic field mixing can result in the apportioning of a finite radiative rate and thus the appearance of a line that would otherwise not exist. The intensity of the new line depends on the mixing and thus on the magnetic field.

Magnetic field induced mixing and the appearance of otherwise forbidden transitions is known from highly charged heliumlike ions, where mixing of the $1s2p\ ^3P_1$ and $1s2p\ ^3P_0$ levels results in the x-ray decay of the $1s2p\ ^3P_0$ level to the $1s^2\ ^1S_0$ ground state, an otherwise strictly forbidden transition. In this case the magnetic field is produced by the nucleus and thus is internal to the ion and very large. Moreover, the $^3P_0$ and $^3P_1$ levels are so close that the magnetic field induced x-ray decay has only been indirectly observed, e.g., by radiative rate measurements [13–16], and cannot be used for plasma diagnostics.

Because of their significance for many high-temperature plasmas [6–8,10,17] we developed our magnetic field sensitive x-ray–line diagnostic for neonlike ions. The closed-shell nature of the $1s^2 2s^2 2p^6\ ^1S_0$

ground state in neonlike ions requires that all transitions involve core-excited levels. The two levels that are particularly suited for magnetic field mixing are the $(1s^2 2s^2 2p^5_{1/2} 3s)_{J=0}\ ^3P_0$ level and the close-by $(1s^2 2s^2 2p^5_{1/2} 3s_{1/2})_{J=1}\ ^1P_1$ level (cf. Figure 1). The $^3P_0$ level in the absence of an external field is strictly forbidden to decay to the $^1S_0$ ground state. It decays instead via a magnetic dipole ($M1$) transition to the $(1s^2 2s^2 2p^5_{3/2} 3s_{1/2})_{J=1}\ ^3P_1$ level, as illustrated in Fig. 1. But because of the small energy separation it does so only very weakly. By contrast, the neighboring $(1s^2 2s^2 2p^5_{1/2} 3s_{1/2})_{J=1}\ ^1P_1$ level rapidly decays to the ground state via an electric-dipole transition, commonly labeled $3F$. Mixing with the $^1P_1$ level allows the $^3P_0$ to decay to the $^1S_0$ ground state with a finite, albeit small, radiative rate. Although closeness is a prerequisite for mixing, the two levels are sufficiently far apart so that the presence of a line resulting from the magnetic field induced x-ray decay of the $(2p^5_{1/2} 3s_{1/2})_{J=0}\ ^3P_0$ level can be observed and resolved from the x-ray decay of the neighboring $^1P_1$ level even if the lines were broadened by ion motion.

To assess the amount of mixing, we note that the magnetic field induced Zeeman coupling parameter h links the radiative rate $A_r(^3P_0)$ of the $^3P_0$ decay to the ground state to the radiative rate $A_r(^1P_1)$ of the $^1P_1$ decay to the ground state [12],

$$A_r(^3P_0) = \left(\frac{h}{\Delta E}\right)^2 A_r(^1P_1). \tag{1}$$

Here ΔE is the energy separation of the two levels. The coupling parameter is given by the coupling of the matrix elements

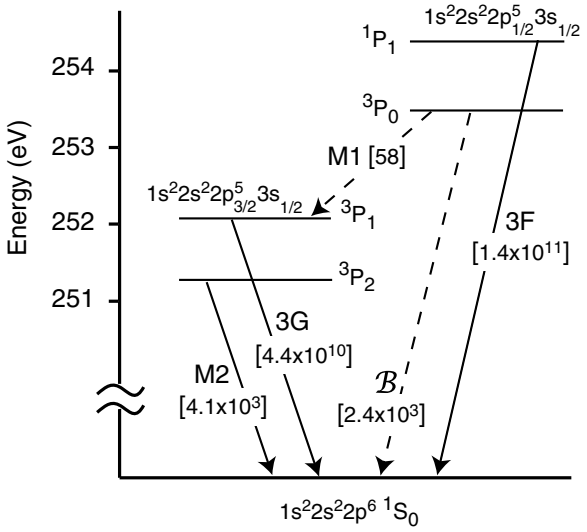

FIG. 1. Grotrian diagram showing the lowest four excited levels in Ar^{8+}. Calculated radiative transition rates (in units of s^{-1}) are indicated in square brackets. The rate for the magnetic field induced line labeled $\mathcal{B}$ assumes a 3-T field.

$$h = \langle ^3P_0 | e \frac{\boldsymbol{\alpha}(\mathbf{r}\times\mathbf{B})}{2} | ^1P_1 \rangle, \tag{2}$$

where e is the electron charge, α is the vector Dirac matrix, and r is the radial position vector. Despite field mixing this coupling will vanish in strict LS coupling if the triplet and singlet states are pure. The $^1P_1$ state, however, is not a pure singlet state but mixes strongly with the $(1s^2 2s^2 2p^5_{3/2} 3s_{1/2})_{J=1}\ ^3P_1$ level (cf. Figure 1). In fact, direct magnetic coupling between the $(1s^2 2s^2 2p^5_{3/2} 3s_{1/2})_{J=1}\ ^3P_1$ and the $^3P_0$ level must also be taken into account. We used a modified GRASP computer code [18] to calculate $A_r(^1P_1) = 1.4 \times 10^{11}\ s^{-1}$ and $A_r(^3P_1) = 4.4 \times 10^{10}\ s^{-1}$. For a splitting $\Delta E \approx 0.9$ eV and $B = 3$ T, the standard field in an electron beam ion trap [19], we obtain $A_r(^3P_0) = 2.44 \times 10^3\ s^{-1}$. This is much larger than the calculated rate for $M1$ decay of the $^3P_0$ level to the $^3P_1$ level of $A_r(M1) = 58\ s^{-1}$. This means the magnetic field induced line should be readily observed in our device. Furthermore, the magnitude of the observed $^3P_0$ x-ray line, labeled $\mathcal{B}$ in Fig. 1, relative to that of the $3F$ line should vary as a function of the magnetic field, as the latter is unaffected by the magnetic field.

Our measurements were performed using the EBIT-II electron beam ion trap, which upon completion in 1990 was the second electron beam ion trap put into use. The Ar^{8+} L-shell x-ray emission was monitored using a grazing-incidence spectrometer with a 2400 ℓ/mm grating and a cooled charged-coupled device (CCD) camera [20]. The instrument affords a resolving power of about 300. Ar^{8+} is produced at an electron energy of 143 eV and ionizes at 423 eV. Because a minimum of about 265 eV is required to collisionally excite the $3s \rightarrow 2p$ transitions, we operated the device at beam energies of 300–400 eV.

Like the first electron beam ion trap, EBIT-I, and several subsequent copies at other laboratories [21], EBIT-II operates at a magnetic field of 3 T. To illustrate the magnetic field sensitivity of the $\mathcal{B}$ x-ray line we have modified the machine operating conditions and successfully operated the device with magnetic fields as low as 1 T.

Spectra obtained at high and low magnetic fields are shown in Fig. 2. The magnetic field induced $^3P_0 \rightarrow {}^1S_0$ x-ray line at 3 T is readily apparent among the other, well-known $3s \rightarrow 2p$ transitions. Using the K-shell lines of heliumlike and hydrogenlike carbon and nitrogen recorded in separate measurements as reference lines, we determined the $^3P_0$–$^1P_1$ splitting to be $\Delta E = 0.895 \pm 0.033$ eV.

The intensity of the $^3P_0$ x-ray line relative to that of the $^1P_1$ line as a function of the square of the magnetic field is shown in Fig. 3. The intensity ratio of the two lines is given by

$$\frac{I_{\mathcal{B}}}{I_{3F}} = I_{\text{inf}} \frac{A_r(^3P_0)}{A_r(^3P_0) + A_r(M1)}. \tag{3}$$

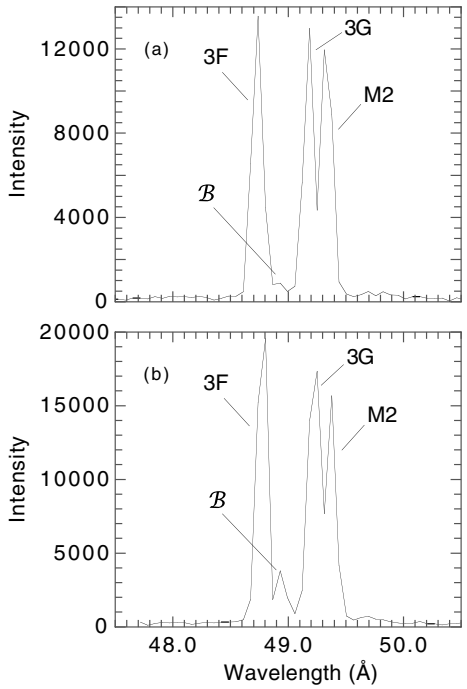

FIG. 2. Spectra of the Ar^{8+} $3s \rightarrow 2p$ emission for different magnetic field values: (a) $B = 1.1$ T, (b) $B = 3.0$ T.

It should drop to half of the high-field value I_{inf} when the field induced and the $M1$ rates are equal. This happens at $B = 0.8$ T, as illustrated by the dashed line in Fig. 3. This is not observed. The halfway point is instead observed at about ten times this value. The reason for the discrepancy is the fact that the $^3P_0$ level is subject to collisional depopulation. Adding the effect of collisions, the intensity ratio is

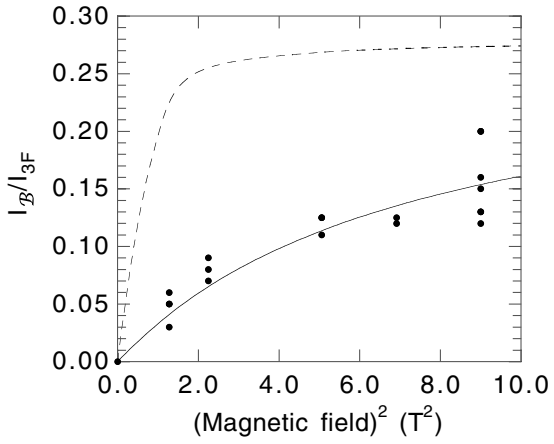

FIG. 3. Intensity of the magnetic field induced line $\mathcal{B}$ relative to that of the $3F$ line as a function of the square of the applied magnetic field. The solid line represents a fit of the experimental ratios (solid circles) assuming an effective electron density of 0.7×10^{11} cm^{-3} and a high-field limit $I_{\text{inf}} = 0.28$. The dashed curve represents the predicted field dependence in the zero-density limit.

$$\frac{I_{\mathcal{B}}}{I_{3F}} = I_{\text{inf}} \frac{A_r(^3P_0)}{A_r(^3P_0) + A_r(M1) + \sigma v n}. \quad (4)$$

Employing the Hebrew University Lawrence Livermore Atomic Code (HULLAC) [22] to calculate the electron-impact excitation cross sections of neonlike Ar^{8+} we find the rate coefficient $\sigma v = 2.78 \times 10^{-8}$ cm^3/s for depopulating the $^3P_0$ level at an electron energy of 400 eV. The magnetic field variation of $I_{\mathcal{B}}/I_{3F}$ using this value for the rate coefficient and a density of 0.7×10^{11} cm^{-3} and $I_{\text{inf}} = 0.28$ is shown by the solid line in Fig. 3. The values for the density and I_{inf} were adjusted until the best fit to the data was obtained. The value of the density required to achieve the best fit in Fig. 3 roughly agrees with the value of 1.3×10^{11} cm^{-3} inferred from the beam parameters of the measurement and assuming a beam ion overlap factor of 0.10.

We note that the electron density can also be inferred from the ratio I_{M2}/I_{3G} of the intensities of the x-ray lines emanating from the $^3P_2$ and $^3P_1$ levels (cf. Figure 1) [10,17]. The average measured ratio $I_{M2}/I_{3G} = 0.88 \pm 0.03$ is consistent with an electron density of 1×10^{11} cm^{-3}.

We tested for the density dependence of $I_{\mathcal{B}}/I_{3F}$ by changing the current and thus the electron density in our device. We were able to lower the density by almost an order of magnitude and still record sufficient signal, as illustrated in Fig. 4. At the lowest density, the measured value for $I_{\mathcal{B}}/I_{3F}$ was 0.27 ± 0.03. These measurements confirmed the zero-density, high-field limit of $I_{\mathcal{B}}/I_{3F}$ we inferred from Fig. 3.

By contrast, the value of the zero-density, high-field limit of $I_B/I_{3F} = 0.28$ does not agree with our calculations. The value of I_{inf} is given by the ratio of the effective excitation rates (i.e., the sum of direct electron-impact excitation and radiative cascades) populating the $^3P_0$ and

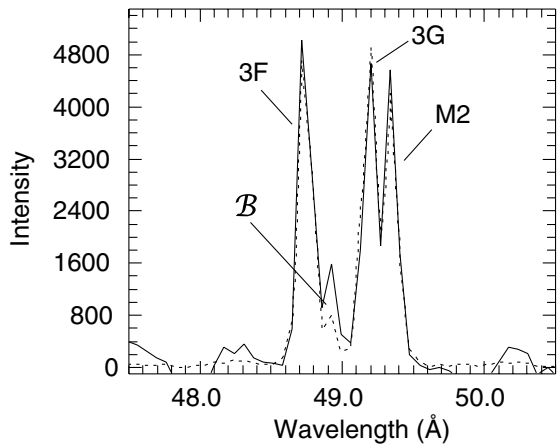

FIG. 4. Spectra of the Ar^{8+} $3s \rightarrow 2p$ emission for different electron densities. Dashed curve: $n \approx 4 \times 10^{10}$ cm^{-3}; solid curve: $n \approx 1.25 \times 10^{10}$ cm^{-3}. This is approximately 2.5 and 8 times less, respectively, than in Fig. 2.

$^1P_1$ upper levels. The HULLAC calculations predict $I_{\text{inf}} = 0.071$. This value is four times smaller than inferred from the data in Fig. 3. Part of the discrepancy stems from the fact that the $\mathcal{B}$ line (an $m_j = 0 \rightarrow m_j = 0$ transition) is fully polarized in the present observation geometry. We observed the line perpendicular to the magnetic field direction. This enhances the emission by a factor of 3/2. Taking this effect into account still leaves nearly a factor of 3 discrepancy. Predicting the intensity of the $3s \rightarrow 2p$ transitions, even with the most sophisticated collisional-radiative models, has been very difficult. Discrepancies between theory and measurement within a factor of 2 are common [23]. The present result confirms and illustrate this.

In the absence of collisions, the diagnostic utility of the magnetic field induced $^3P_0$ decay is largest when the field induced rate and the $M1$ rate are equal. While for Ar^{8+} this happens at $B = 0.8$ T, we calculated that for neonlike Fe^{16+} equality is achieved at 4.7 T. We observed line $\mathcal{B}$ in Fe^{16+} with our apparatus at the highest field setting of 3 T. We also observed line $\mathcal{B}$ in S^{6+}. Line $\mathcal{B}$ is produced in neonlike sulfur already at a few thousand G and, therefore, is prominent even at the lowest magnetic field values we could attain in our device.

By observing the $\mathcal{B}$ line in neonlike ions of different atomic number, magnetic field strengths may be measured over a wide range and for different plasma temperatures. We note that the principle of magnetic field mixing of allowed and forbidden lines may be generalized to other appropriate atomic systems, e.g., nickel-like ions.

The diagnostic may also be used in high-density plasmas. For example, the magnetic fields in Z pinches may reach 1–10 kT. Because of the quadratic dependence of the field induced rate on the magnetic field in Eq. (2) the value of $A_r(^3P_0)$ is 6 to 8 orders of magnitude larger than in our device. Therefore, $A_r(M1)$ is negligible by comparison and can be dropped from Eq. (4). In this case, $A_r(^3P_0)$ competes with the collisional quenching rate $\sigma v n$ at densities in the range 10^{17}–10^{21} cm^{-3}. The magnetic field strength can then be inferred from the value of $I_{\mathcal{B}}/I_{3F}$ and an independent measurement of the electron density.

In summary, we have shown that the ratio of the $^3P_0 \rightarrow {}^1S_0$ and $^1P_1 \rightarrow {}^1S_0$ L-shell x-ray lines in neonlike Ar^{8+} is a diagnostic of the magnetic field strength, especially in low-density plasmas where $n < 5 \times 10^{10}$. Moreover, the principle behind the line diagnostic can readily be generalized to other neonlike ions and other ionic systems. It will therefore be possible to select an ionic system at a given temperature for determining a particular range of magnetic field strengths. This new spectral diagnostic therefore promises to be a key for resolving models concerning the evolution, generation, and effects of magnetic fields in high-temperature laboratory and astrophysical plasmas where direct magnetic field measurements were so far impossible.

We thank Dr. J. Bailey at the Sandia National Laboratory, Dr. J. Lepson at the University of California Berkeley, and Dr. M. Foord at the Lawrence Livermore National Laboratory for stimulating discussions. This work was supported by Work Order No. W-19 878 from NASA's Space Research and Analysis Program and performed by the University of California Lawrence Livermore National Laboratory under the auspices of the Department of Energy under Contract No. W-7405-Eng-48.

[1] J. O. Stenflo, Rep. Prog. Phys. **41**, 865 (1978).
[2] C. M. Johns-Krull, J. A. Valenti, and C. Koresko, Astrophys. J. **516**, 900 (1999).
[3] M. Tatarakis *et al.*, Nature (London) **415**, 280 (2002).
[4] A. S. Sandhu *et al.*, Phys. Rev. Lett. **89**, 225002 (2002).
[5] C. De Michelis and M. Mattioli, Nucl. Fusion **21**, 677 (1981).
[6] B. A. Hammel *et al.*, Phys. Rev. Lett. **70**, 1263 (1993).
[7] C. R. Canizares *et al.*, Astrophys. J. **539**, L41 (2000).
[8] A. P. Rasmussen *et al.*, Astron. Astrophys. **365**, L231 (2001).
[9] J. Sanz-Focada, N. S. Brickhouse, and A. K. Dupree, Astrophys. J. **554**, 1079 (2001).
[10] C. W. Mauche, D. A. Liedahl, and K. B. Fournier, Astrophys. J. **560**, 992 (2001).
[11] P. Zeeman, Philos. Mag. **43**, 226 (1897).
[12] R. D. Cowan, *The Theory of Atomic Structure and Spectra* (University of California Press, Berkeley, 1981).
[13] R. Marrus *et al.*, Phys. Rev. Lett. **63**, 502 (1989).
[14] P. Indelicato and E. Lindroth, Phys. Rev. A **46**, 2426 (1992).
[15] K. L. Wong *et al.*, Phys. Rev. A **51**, 1214 (1995).
[16] E. G. Myers *et al.*, Phys. Rev. Lett. **76**, 4899 (1996).
[17] M. Klapisch *et al.*, Phys. Lett. **69A**, 34 (1978).
[18] F. A. Parpia, C. F. Fischer, and I. P. Grant, Comput. Phys. Commun. **94**, 249 (1996).
[19] R. E. Marrs *et al.*, Phys. Rev. Lett. **60**, 1715 (1988).
[20] S. B. Utter *et al.*, Rev. Sci. Instrum. **70**, 284 (1999).
[21] P. Beiersdorfer *et al.*, in *X-Ray and Inner-Shell Processes: Proceedings of the 19th International Conference on X-Ray and Inner-Shell Processes*, CP652, edited by A. Bianconi, A. Marcelli, and N. L. Saini (American Institute of Physics, New York, 2003), pp. 131–140.
[22] A. Bar-Shalom, M. Klapisch, and J. Oreg, J. Quant. Spectrosc. Radiat. Transfer **71**, 169 (2001).
[23] K. J. H. Phillips *et al.*, Astron. Astrophys. **138**, 381 (1999).